tiomeric structure were respectively equal to 0.060 and 0.081, GOF = 2.27.

Synthesis of $C_2Ph_4P_2Li_2$ (2). The dianion was synthesized by treatment of 1,2,3,4-tetraphenyl-1,2-dihydro-1,2-diphosphete (**1**) with 2 equiv of lithium according to the method outlined in ref 5. The product was used as a solution in THF without further purification.

Synthesis of $C_2Ph_4P_2(SiMe_3)_2$ (3). A solution of **2** (5 mmol) in 25 mL of THF was cooled to −78 °C and chlorotrimethylsilane (1.3 mL, 1.1 g, 10 mmol) added dropwise by syringe. The mixture was allowed to stir at −78 °C until the color had faded to orange-yellow, and the $^{31}P\{^1H\}$ NMR spectrum indicated complete formation of the silylated product. The mixture was allowed to attain ambient temperature and the THF removed in vacuo to give a yellow oil which was extracted into 50 mL of a (5:1) hexane–toluene mixture. The resulting suspension was rapidly filtered through Celite and the solvent removed in vacuo from the filtrate to give **3** as a yellow oil which was characterized by ^{31}P NMR spectroscopy and used, without further purification owing to its sensitivity to moisture and air, as a solution (0.1 M) in toluene. $^{31}P\{^1H\}$ (THF): $\delta^{31}P$ −45 ppm.

Synthesis of $[Ni(\eta^2\text{-PhCH=CHPh})(PR_3)_2]$. $[NiCl_2(PR_3)_2]$ (1 mmol) was suspended in a toluene solution of *trans*-stilbene (200 mg, 1.1 mmol, in 30 mL) and cooled to 0 °C. SuperHydride (2 mL, 2 mmol) was added dropwise by syringe and the mixture allowed to stir at 0 °C for 5 min. During this time the suspended nickel starting complex dissolved, the color changed from deep red to a yellow-brown, and a gas was evolved. The mixture was allowed to attain ambient temperature (5 min), and the formation of the η^2-nickel(0) complex was verified by ^{31}P NMR spectroscopy. The mixture was subsequently cooled to −78 °C and used immediately. $^{31}P\{^1H\}$: δP (THF) +42 (DPPE), +22 ($PPh(CH_2Ph)_2$, +17 (PEt_3), +9 (DPPP), +8 (P^nBu_3), −3 (PMe_2Ph).

Synthesis of $[Ni(C_2Ph_4P_2)(PR_3)_2]$. (a) $[NiCl_2(PR_3)_2]$ (2 mmol) was suspended in toluene (30 mL) and cooled to 0 °C. **3** (2 mmol) was added dropwise as a toluene solution (20 mL) causing the dissolution of the suspended nickel(II) complex. The solvent was removed in vacuo and the residue washed with cold hexane (3 × 5 mL at −78 °C). The residue was dissolved in a minimum of toluene and the complex precipitated with hexane ($PR_3 = {}^1/_2DPPE$, $PPh(CH_2Ph)_2$). $^{31}P\{^1H\}$ NMR (toluene): (**4**) +89, +52 (AA′XX′, $\sum J_{AX} + J_{AX'} = 88$); (**5**) +131, +35 ($A_2X_2$, $^2J_{PNiP} = 42$); (**6a**) +89, +51 (AA′XX′, $\sum J_{AX} + J_{AX'} = 98$); (**7**) +106, −3 ($A_2X_2$, $^2J_{PNiP} = 51$); (**8a**) +90, +52 (AA′XX′, $\sum J_{AX} + J_{AX'} = 94$); (**9a**) +89, +52 (AA′XX′, $\sum J_{AX} + J_{AX'} = 98$). $^{13}C\{^1H\}$ NMR (CD_2Cl_2): (**4**) 1.3 (m, CH_2), 155.2 (d, $^1J_{PC} = 47$ Hz, =*C*—P). ^1H NMR (CD_2Cl_2): (**4**) 2.11 (4 H, b, CH_2), 6.9–7.7 (40 H, m, Ph). Mass spectra (EI, 70 eV): (**4**) *m/z* 849 ($M^+ - H$, 10%), 398 ($Ph_2PCH_2CH_2PPh_2^+$, 87%), 394 ($C_2Ph_4P_2^+$, 100%).

(b) To a toluene solution of $[Ni(\eta^2\text{-PhCH=CHPh})(PR_3)_2]$ (1 mmol in 30 mL) cooled to −78 °C was rapidly added a toluene solution of $C_2Ph_4P_2$ (395 mg, 1 mmol). The mixture was stirred for 1 min and then examined by ^{31}P NMR spectroscopy. $^{31}P\{^1H\}$ NMR (toluene): (**4**) +89, +52 (AA′XX′, $\sum J_{AX} + J_{AX'} = 88$); (**6b**) +103, +24 ($A_2X_2$, $^2J_{PNiP} = 49$); (**7**) +106, −3 (A_2X_2, $^2J_{PNiP} = 51$); (**8b**) +113, +19 (A_2X_2, $^2J_{PNiP} = 48$); (**9b**) +114, +11 (A_2X_2, $^2J_{PNiP} = 49$). $^{13}C\{^1H\}$ NMR (CD_2Cl_2): (**4**) 1.3 (m, CH_2), 155.2 (d, $^1J_{PC} = 47$ Hz, =*C*—P). ^1H NMR (CD_2Cl_2): (**4**) 2.11 (4 H, b, CH_2), 6.9–7.7 (40 H, m, Ph).

Synthesis of $[Pt(C_2Ph_4P_2)(PPh_3)_2]$ (11). $[Pt(C_2H_4)(PPh_3)_2]$ (148 mg, 0.2 mmol) and **1** (80 mg, 0.2 mmol) were separately dissolved in 3 mL of toluene and cooled to 0 °C. The solution and the platinum(0) complex was added to the solution of **1** by transfer wire, a reaction occurring immediately with the evolution of a gas to give a deep red solution. The solvent was removed in vacuo and the residue washed with hexane (2 × 5 mL) to give an orange-red solid. $^{31}P\{^1H\}$ NMR (toluene): δP ($C_2Ph_4P_2$) +77 ($^1J_{PtP} = 1512$); δP (PPh_3) +29 ($^1J_{PtP} = 3122$; $\sum J_{AX} + J_{AX'} = 132$).

Supplementary Material Available: Tables of crystallographic data, positional and displacement parameters, and bond distances and angles (25 pages); tables of observed and calculated structure factors (58 pages). Ordering information is given on any current masthead page.

Electrochemical Synthesis of Ceramic Materials. 2. Synthesis of AlN and an AlN Polymer Precursor: Chemistry and Materials Characterization

Travis Wade, Jongman Park, Ernest Gene Garza, Claudia B. Ross, Douglas M. Smith, and Richard M. Crooks*

Contribution from the UNM/NSF Center for Micro-Engineered Ceramics, University of New Mexico, Albuquerque, New Mexico 87131. *Received June 26, 1992*

Abstract: A simple electrochemical method for the preparation of AlN and other metal nitride ceramic precursors is described. Constant-current electrolysis in a cell containing a NH_4Br/NH_3 electrolyte solution and Al electrodes yields a solid mixture consisting primarily of $Al(NH_3)_6Br_3$ and $[Al(NH_2)(NH)]_n$ after excess NH_3 is removed. Calcination of this mixture above 600 °C in flowing NH_3 results in elimination of $Al(NH_3)_6Br_3$ and conversion of the AlN polymer precursor, $[Al(NH_2)(NH)]_n$, to high surface area AlN powder containing low levels of oxygen and carbon impurities. In this report, some electrochemical aspects of the AlN polymer precursor synthesis and processing are discussed. Characterization of the AlN powder before and after sintering is also discussed.

Introduction

In this paper, we discuss a new electrochemical method for synthesizing an inorganic AlN polymer precursor. Metal nitride ceramics represent an important area of research at the present time, because they often have superior electronic, thermal, or mechanical characteristics compared to those of the corresponding oxides. For example, compared to Al_2O_3, AlN has much higher thermal conductivity, a better thermal expansion match to Si, lower electrical conductivity, comparable mechanical strength, and optical properties that are suitable for optoelectronics applications in some cases.[1-3] However, metal nitride ceramics have not as yet found widespread commercial applications, because they are generally more challenging and costly to synthesize and process than oxides. The purpose of this paper is to introduce a new synthetic method that yields an AlN polymer precursor, which can be calcined at relatively low temperature to yield pure-metal or mixed-metal nitride ceramics with desirable morphological and compositional characteristics. We have chosen to focus this paper

* Author to whom correspondence should be addressed.

(1) Sheppard, L. M. *Am. Ceram. Soc. Bull.* **1990**, *69*, 1801.
(2) Kuramoto, N.; Taniguchi, H. *J. Mater. Sci. Lett.* **1984**, *3*, 471.
(3) Marchant, D. D.; Nemecek, T. E. *Adv. Ceram.* **1989**, *26*, 19.

0002-7863/92/1514-9457$03.00/0

Scheme I. Proposed In-Cell Chemistry Leading to Formation of AlN

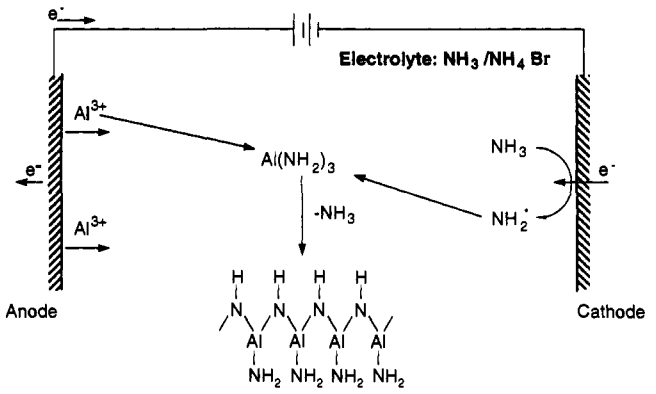

Table I. Electrode Reactions in the Cell: Al/NH_3, NH_4^+, Br^-/Al

Cathode Reactions	
$e^-(Al) \rightarrow e_s^-$	(3)
$NH_4^+ + e^- \rightarrow NH_3 + {}^1/_2H_2$	(4)
$NH_3 + e^- \rightarrow NH_2^- + {}^1/_2H_2$	(5)
Anode Reactions	
$4NH_3 \rightarrow {}^1/_2N_2 + 3NH_4^+ + 3e^-$	(6)
$Br^- \rightarrow {}^1/_2Br_2 + e^-$	(7)
$Al \rightarrow Al^{3+} + 3e^-$	(8)
$e_s^- \rightarrow e^-(Al)$	(9)

on AlN, since its high theoretical thermal conductivity, 320 W/(m K), and its high electrical resistivity, $>10^{13}$ Ω cm, make it of commercial interest as an electronics packaging material.[1-3] However, we have also used electrochemical methods to synthesize TiN, NbN, and Zn_3N_2, as well as mixtures of AlN and TiN.

Commercial AlN powder is presently made by direct nitridation of Al (eq 1) or by carbothermal reduction of alumina (eq 2).[1-3]

$$N_2 + 2Al \rightarrow 2AlN\ (1200\text{–}1400\ °C) \quad (1)$$

$$Al_2O_3 + 3C + N_2 \rightarrow 2AlN + 3CO\ (1200\text{–}1750\ °C) \quad (2)$$

Thin films are made by polymer pyrolysis or by chemical vapor deposition (CVD).[1-5]

We recently presented a preliminary report of an electrochemical route for the preparation of metal nitride ceramic precursors in NH_4Br/NH_3 electrolyte solutions.[6] The process is similar to previously reported homogeneous[7] and heterogeneous[8] metal nitride ceramic precursor syntheses, but the electrochemical approach described here is more easily implemented, requires only inexpensive starting materials, yields nitride powders containing lower carbon and oxygen impurity levels, and does not result in the formation of any unrecoverable or noxious byproducts. Moreover, preliminary characterization of the resulting AlN powder indicates high surface area and chemical stability, suggesting that it will densify at a significantly lower temperature than powders synthesized by alternative routes and that it may be useful as a catalyst support.

Scheme I illustrates the processes that we believe are responsible for AlN polymer precursor formation. The anode and cathode reactions shown in Scheme I are known to occur in liquid NH_3, as are the other reactions shown in Table I.[7,9,10] The product

Scheme II. Proposed Homogeneous Chemistry Leading to Formation of AlN from an Electrosynthesized Precursor[a]

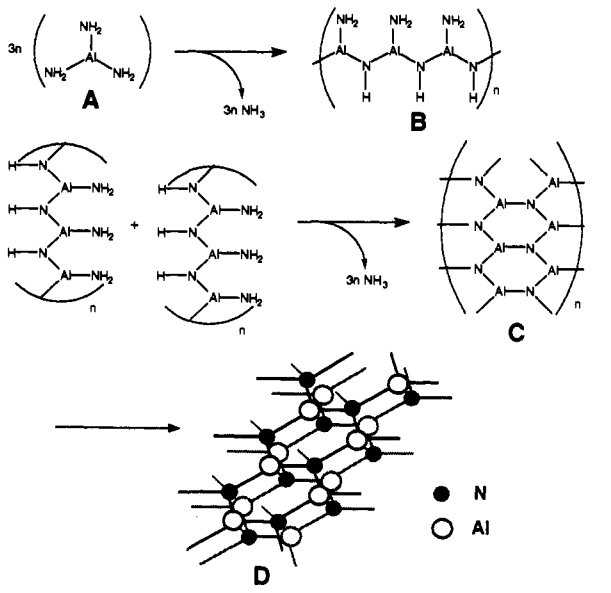

[a] NMR data indicate that Al in species B is coordinated to three NH_3 molecules. Species D is AlN.

that results from reaction between Al^{3+} and NH_2^- in NH_3 solvent, $Al(NH_2)_3$, is also known.[7,9] $Al(NH_2)_3$ can undergo NH_3 condensation at room temperature to produce AlN polymer precursors of the general form $[Al(NH_2)NH]_n$, and further NH_3 condensation at elevated temperature results in AlN (Scheme II).[7,11]

We are interested in the effect of electrochemical and processing variables on electrosynthesized polymeric ceramic precursors and AlN purity, yield, and morphology. Information about these relationships will permit us to identify the electrosynthetic reaction pathway responsible for the AlN polymer precursor, maximize the cell current efficiency, and control the chemical and morphological characteristics of the ceramic powders. The first part of this paper addresses issues related to the electrochemical synthesis of the AlN polymer precursor, $[Al(NH_2)(NH)]_n$, and the second part is concerned with powder processing.

Experimental Section

Precursor Synthesis. Electrochemical reactions were carried out using two separate single-compartment, two-electrode cell configurations. The first cell had a solution volume of 75 mL and was used primarily for experiments in which we wished to achieve limiting electrochemical behavior on a rapid time scale. The second cell had a solution volume of 300 mL and was useful for synthesizing quantities of powder sufficient to satisfy materials characterization needs.

The 75-mL cell has been described previously.[6] Briefly, the cell was glass and configured for vacuum-line electrochemistry. It contained two 0.05-cm-thick Al electrodes (Johnson-Mathey, 99.998%), typically 12.5 cm^2/side, oriented parallel to each other and spaced by about 1 cm. The electrodes were rinsed in ethanol and water prior to electrolysis. The 300-mL cell was essentially a larger version of the 75-mL cell; however, it employed concentric cylinder Al electrodes of the same thickness which were separated by about 0.5 cm. The anode was the outer cylinder and had an approximate area of 76 cm^2/side. The cathode area was about 64 cm^2/side. All current densities are based on the area of a single side of the anode. The 300-mL cell configuration allowed us to synthesize about 4–5 g of AlN per electrolysis.

The electrosynthesis was performed identically in both cells. Reagent-grade NH_4Br (Merck) was dried for 1 h in a vacuum oven at 80 °C and then added to the cell to make the final concentration 0.05–0.7 M. NH_4Br was the electrolyte of choice for the following reasons: (1) it is soluble in NH_3 at −78 °C; (2) it does not contain O or C; (3) its elec-

(4) Interrante, L. V.; Lee, W.; McConnell, M.; Lewis, N.; Hall, E. *J. Electrochem. Soc.* **1989**, *136*, 472.
(5) Jiang, Z.; Interrante, L. V. *Chem. Mater.* **1990**, *2*, 439.
(6) Ross, C. B.; Wade, T.; Crooks, R. M.; Smith, D. M. *Chem. Mater.* **1991**, *3*, 768.
(7) Maya, L. *Adv. Ceram. Mater.* **1986**, *1*, 150.
(8) (a) Rüssel, C.; Seibold, M. M. *J. Am. Ceram. Soc.* **1989**, *72*, 1503. (b) Seibold, M.; Rüssel, C. *Mater. Res. Soc. Symp. Proc.* **1988**, *121*, 477. (c) Rüssel, C. *Chem. Mater.* **1990**, *2*, 241.
(9) Nicholls, D. *Inorganic Chemistry in Liquid Ammonia*; Elsevier: Amsterdam, The Netherlands, 1979; pp 50–52.
(10) Maya, L. Aluminum Electrochemistry in Liquid Ammonia. Report ORNL/TM-9762; Oak Ridge National Laboratory: Oak Ridge, TN, 1985.

(11) Results from ^{27}Al MAS NMR indicate that all Al in the precursor powder is 6-coordinate prior to calcining but 4-coordinate after calcining in NH_3 for 2 h at temperatures above 600 °C. This suggests that Al in $[Al(NH_2)(NH)]_n$ is further ligated to three NH_3 molecules. See ref 9, pp 70–72, 158.

trolysis products do not appear to adversely affect the resulting AlN powder. (Caution: Electrolysis of NH_3 solutions containing I^- salts can result in formation of dangerous levels of NI_3.) The cell was attached to a glass, diffusion-pumped vacuum line and evacuated to a pressure of $1-5 \times 10^{-4}$ mmHg. Anhydrous-grade NH_3 (Matheson) was purified by condensation onto Na at reduced pressure, followed by 1 or 2 freeze–pump–thaw cycles, prior to being distilled into the electrochemical cell.[12,13]

Electrolyses were performed at constant current for various lengths of time using a Sorensen Model DCR 150-3B current source (Raytheon Co.). Current densities were 270 A/m^2 in the 75-mL cell and 260 A/m^2 in the 300-mL cell. The temperature of the electrolyte solution was not monitored, but the cell was immersed in a dry ice/isopropanol bath at −78 °C during each electrolysis. Cell voltage was measured between the anode and cathode using a Dana Model M5900 digital multimeter and recorded as a function of time on a Kipp and Zonen Model BD-90 X-Y recorder. During each electrolysis, an insoluble white material, presumably the AlN polymer precursor and $Al(NH_3)_6Br_3$, precipitated in the electrolyte solution and on the Al electrodes.

Following each electrolysis, NH_3 was allowed to evaporate from the cell through a Hg manometer. Residual NH_3 was removed by overnight vacuum evacuation of the cell at 25 °C. Finally, the cell was disconnected from the vacuum line and placed in a N_2-containing drybox.

The powder remaining in the cell after electrolysis was collected by scraping it off the cell walls and electrodes, and then it was transferred to quartz boats for subsequent calcination.

Here, we use "precursor powder" to refer to all species present in the powder immediately following electrolysis and "AlN polymer precursor" to refer to $[Al(NH_2)(NH)]_n$, the species which yields AlN upon calcination.

Calcination and Hot Pressing. Quartz boats containing the solid material from the electrochemical cell were loaded into a gas-tight quartz tube and then removed from the N_2-containing drybox. The tube was placed in a calibrated Lindberg Model 55035 tube furnace, and the powder was exposed to flowing gas (600 mL/min), usually NH_3, that was prepurified by passing it over finely dispersed Na metal.[13] The calcining protocol was as follows: heat at 5 °C/min to the maximum temperature, hold for 2 h, and then cool to 25 °C at 10 °C/min. Following calcination, the tube was returned to the drybox, and the AlN was removed, weighed, and stored for subsequent analysis.

Powder specimens were uniaxially hot-pressed for 1–2 h in an O_2-gettered Ar atmosphere using BN-lined graphite dies.

Materials Characterization. A. Elemental Analysis. Most elemental analyses were performed by Galbraith Laboratories, Inc. (Knoxville, TN). C and H were analyzed using a Leco Model 800 elemental analyzer. Br was analyzed by thiosulfate titration. AlN was digested in $LiBF_4$, and the Al was determined by inductively coupled plasma spectroscopy. N was determined by ignition of the AlN powder in O_2 at 1000 °C, reduction of the resulting vapor over a Cu catalyst, and then quantitative analysis by thermal conductivity.

B. FTIR. FTIR analyses were performed using a Bomem Model MB-100 FTIR spectrophotometer (4 cm^{-1} resolution, DTGS detector). Samples were prepared as KBr pellets in a N_2-containing drybox. Authentic samples of $Al(NH_3)_6Br_3$ were prepared by exposing $AlBr_3$ to NH_3 liquid or vapor at low pressure.[14]

C. NMR. ^{27}Al MAS NMR spectroscopy was performed on a Varian Unity 1 spectrometer at an applied field strength of 9.4 T and a nominal resonance frequency of 104 MHz. Finely ground powders were loaded into zirconia rotors in a N_2-containing drybox. A 9-kHz spinning speed was used to minimize the effects of spinning sidebands. Chemical shifts are referenced to 1 M $AlCl_3$ in water. Coordination symmetry was determined by comparison to authentic samples of $Al(NH_3)_6Br_3$ and AlN.

D. Thermal Analysis. TGA analysis of AlN powder stability was performed using an Omnitherm Model STA 1500 TGA/DTA instrument (Stanton Redcroft Ltd.).

E. Morphological Analysis. Surface areas were determined by nitrogen adsorption at 77 K. The BET analysis employed a molecular cross sectional area of 0.162 nm^2 and five relative pressures in the range 0.05–0.35. Prior to analysis, samples were outgassed under vacuum at 110 °C for 5 h. All measurements were made with an Autosorb-1 static volumetric analyzer. Skeletal densities were measured by He displacement at 25 °C by using a Quantachrome micropycnometer. Electron micrographs of Pt-coated samples were obtained using a Hitachi Model S-800 scanning electron microscope.

F. XRD. X-ray powder diffraction spectra were obtained with a Scintag PAD V diffraction system (Cu Kα line, Ni filter, Beryllium window, stepped scan (0.025°/step, 3 s/step)).

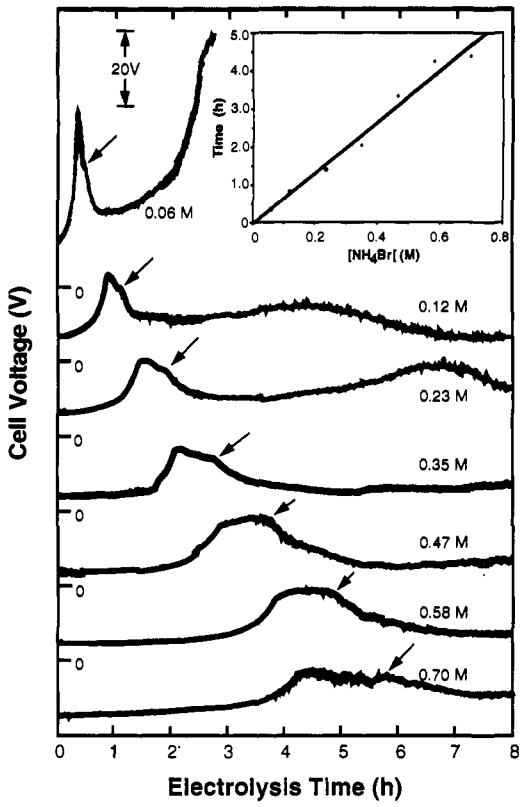

Figure 1. Cell voltage vs electrolysis time for an AlN polymer precursor synthesized using various concentrations of NH_4Br electrolyte. The arrows indicate the time at which the characteristic blue color of e_s^- became persistent throughout the solution, which indicates a significant concentration of e_s^-. Prior to the appearance of the blue color, e_s^- may be generated but rapidly react with NH_4^+. Data were obtained for constant-current electrolyses, 260 A/m^2, in the 300-mL cell. The inset shows the linear relationship between V_{max} and $[NH_4Br]$.

Results and Discussion

Electrochemical Synthesis of AlN. To understand the electrochemical processes that are responsible for the AlN polymer precursor, $[Al(NH_2)(NH)]_n$, we measured the magnitude of the electrochemical cell voltage, V_{cell}, as a function of electrolysis time for different concentrations of NH_4Br electrolyte (Figure 1). For 0.06 M NH_4Br, the potential–vs–time plot indicates rapid attainment of a voltage maximum, V_{max}, after about 30 min, which is followed by a steady increase to the maximum output voltage of the current source after 3 h. Concentrations between 0.1–0.7 M NH_4Br also yield voltage–vs–time curves that have a pronounced V_{max}; but in these cases, V_{max} is smaller, and it is not followed by the large voltage increase. For each plot, V_{max} is accompanied by a shoulder, which typically appears about 30 min after the time corresponding to V_{max}. Just prior to the onset of these shoulders, we noted that the electrolyte solution changed from colorless to deep blue. The blue color is characteristic of solvated electrons, e_s^-, which can be generated in liquid NH_3 electrolyte solutions (eq 3).[15] Concurrent with the generation of e_s^-, we also noted a progressive decrease in the rate of H_2 evolution at the cathode. Once persistent e_s^- are observed in the cell, there is no further evolution of gas.

We interpret the voltage–vs–time plots as follows: The slow initial increase in voltage results from an increase in solution resistance brought about by the cathodic reduction of NH_4^+ (eq 4) and the precipitation of Br^- by electrogenerated Al^{3+}.[9,16] The

(12) Demortier, A.; Bard, A. J. *J. Am. Chem. Soc.* **1973**, *95*, 3495.
(13) Shriver, D. F.; Drezdzon, M. A. *The Manipulation of Air-Sensitive Compounds*, 2nd ed.; Wiley: New York, 1986.
(14) We have chosen to represent the ammoniate of Al^{3+} as $Al(NH_3)_6^{3+}$, because ^{27}Al MAS NMR data indicate that when $AlBr_3$ is exposed to NH_3 vapor at 25 °C and then evacuated overnight, the resulting Al compound is 6-coordinate. However, under other conditions, ammoniated Al^{3+} may be present with a varying number of NH_3 ligands. See ref 9.

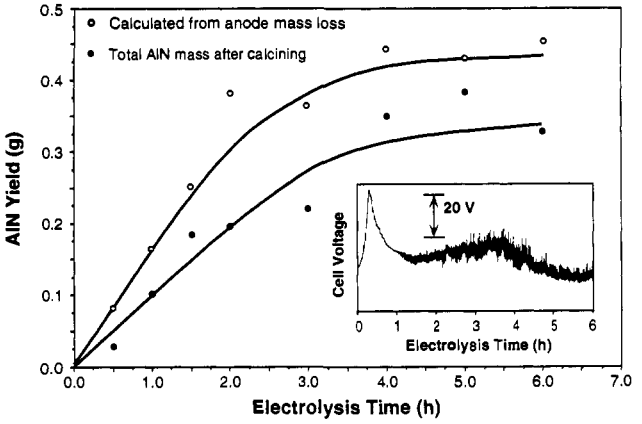

Figure 2. AlN yield vs electrolysis time. The precursor powder was calcined at 1100 °C in flowing NH_3. The inset shows the cell voltage vs time profile for the 6-h electrolysis. Data were obtained for electrolyses in the 75-mL electrolysis cell, which contained 0.06 M NH_4Br and liquid NH_3. The current density was 270 A/m^2. The data represented by filled circles were calculated on the basis of the total AlN recovered from the cell, and the data represented by open circles correspond to the AlN yield calculated from the mass loss of the anode.

absence of NH_4Br after electrolysis is confirmed by FTIR spectroscopic results discussed later.

When the current demand is exceeded by the flux of electrolyte to the cathode, additional heterogeneous reactions occur. Thermodynamically, the lowest energy cathode reactions in this electrochemical cell that do not involve the electrolyte are the generation of e_s^- (eq 3) and formation of NH_2^- (eq 5).[9,15] Initially, both NH_2^- and e_s^- react with NH_4^+ in solution to generate NH_3 or NH_3 and H_2, respectively. After NH_4^+ is consumed, the characteristic blue color of e_s^- is observed, and V_{cell} drops, because e_s^- decreases the solution resistance. This argument is strongly supported by the approximately linear relationship between the time necessary to achieve V_{max} and the electrolyte concentration, as shown in the inset of Figure 1. At this low temperature, we anticipate that the homogeneous reaction between e_s^- and NH_3, to form NH_2^-, will proceed slowly.

Our interpretation of Figure 1 has two important ramifications. First, the electrolysis conditions which result in formation of $[Al(NH_2)(NH)]_n$ also consume electrolyte, thereby lowering overall current efficiency. However, the solution resistance does rise continuously because parasitic electrode reactions generate mobile charge carriers such as e_s^-. Second, e_s^- formed at the cathode are consumed at the anode (eq 9), thereby significantly reducing the overall current efficiency of the electrolysis after the time corresponding to V_{max}.

Characterization and Processing of AlN and Its Polymer Precursor. The AlN yield is related to the time of electrolysis, the initial electrolyte concentration, and the current density. The data in Figure 2 are a plot of AlN yield vs electrolysis time. The mass of AlN synthesized is a linear function of the electrolysis time between 0 and ~2.5 h. However, extended electrolysis does not result in additional yield, suggesting that a critical reactant is not present in the cell after prolonged electrolysis. It is not likely that the concentration of NH_2^- is diminished, since it is formed at about the same potential as e_s^-. Therefore, we conclude that Al oxidation (eq 8) is suppressed, because e_s^- oxidation (eq 9), which occurs at a more negative potential than Al oxidation, becomes an important anode process.

When the mass of electrogenerated AlN is calculated from the Al-anode mass loss, rather than directly from the mass of AlN remaining after calcination, the shape of the yield–vs–time curve is similar to that discussed above, but the calculated yield of AlN is about 25% higher. The difference between the two curves indicates that not all of the oxidized Al takes part in the formation of the AlN polymer precursor. Results obtained from FTIR spectroscopy and ^{27}Al MAS NMR suggest that the parasitic byproduct is ammoniated $AlBr_3$, $Al(NH_3)_6Br_3$ (vide infra).

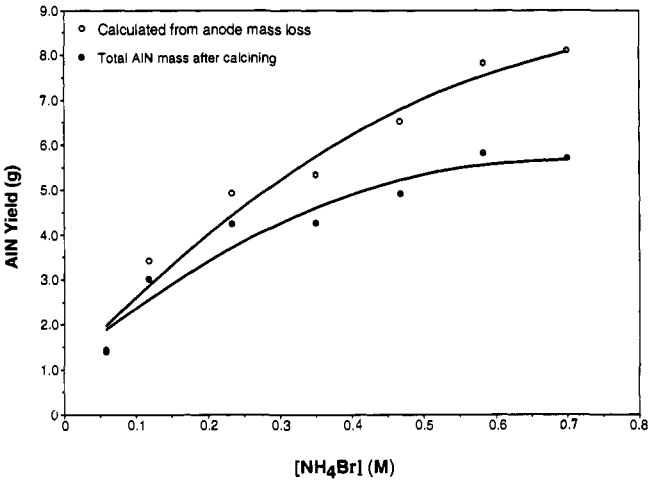

Figure 3. AlN yield vs NH_4Br electrolyte concentration for 8-h electrolyses in the 300-mL cell. The data represented by filled circles were calculated on the basis of the total AlN recovered from the cell, and the data represented by open circles correspond to the AlN yield calculated from the mass loss of the anode.

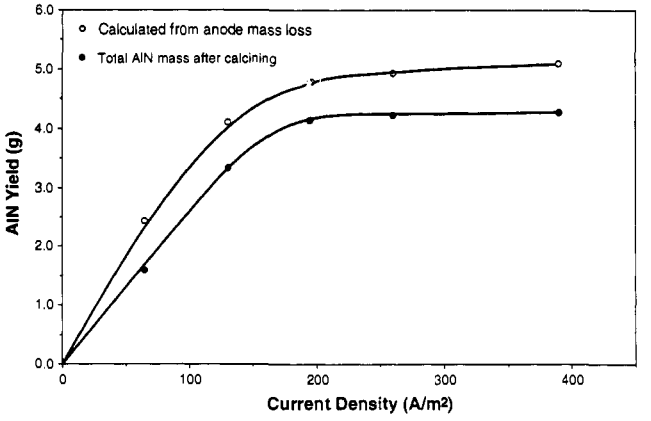

Figure 4. AlN yield vs current density for 8-h electrolyses in the 300-mL cell containing 0.23 M NH_4Br. The data represented by filled circles were calculated on the basis of the total AlN recovered from the cell, and the data represented by open circles correspond to the AlN yield calculated from the mass loss of the anode.

Figure 3 shows that the yield of AlN depends on the initial electrolyte concentration. The data indicate that limiting behavior is not obtained; rather, the AlN yield depends linearly on the concentration of NH_4Br for concentrations above 0.23 M. This suggests that the electrolyte concentration affects one of the AlN polymer precursor reactants. Since the presence of NH_4Br suppresses formation of e_s^-, it is very likely that $[Al(NH_2)(NH)]_n$ formation only occurs in the absence of high concentrations of e_s^-. In other words, the data shown in Figure 3 support our earlier conclusion that e_s^- oxidation (eq 9) prevents Al oxidation and therefore suppresses precursor formation.

Figure 4 shows how the AlN yield relates to the current density. On a per-coulomb basis, higher current densities result in lower AlN yields. This effect also arises from the presence of e_s^-. Higher current densities necessitate higher values of V_{cell} and therefore shift the cathode process more strongly toward e_s^- formation, reducing Al oxidation and suppressing formation of $[Al(NH_2)(NH)]_n$. Note that approximately unit current efficiency for Al oxidation is obtained at the lower current densities.

Figure 5 shows the transmission FTIR spectra obtained for the precursor powder before and after calcining at different temperatures in flowing NH_3. The bottom spectrum, obtained prior to calcination, shows bands at 1307 and 1620 cm^{-1} that are

(15) Teherani, T.; Itaya, K.; Bard, A. J. *Nouv. J. Chim.* **1978**, *2*, 481.
(16) *Chemistry in Nonaqueous Ionizing Solvents*; Jander, G., Spandau, H., Addison, C. C., Eds.; Wiley: New York, 1966; Vol. 1, Part 1, Chapter 2.

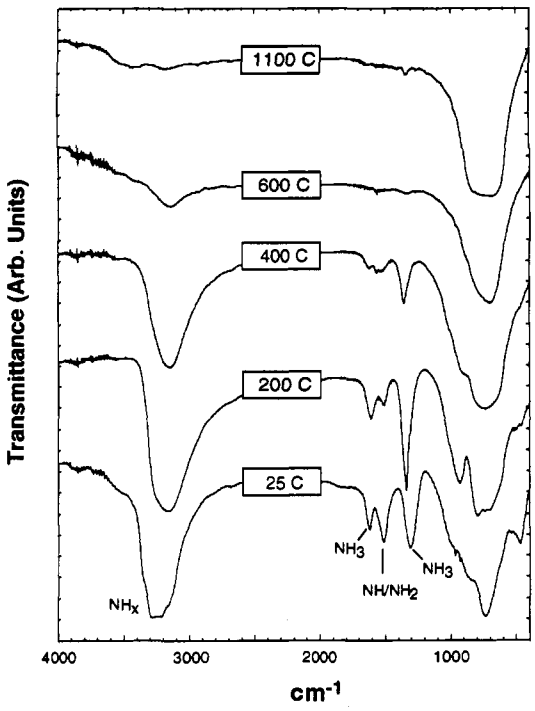

Figure 5. Transmission FTIR spectra for an electrosynthesized precursor powder before and after calcining at various temperatures in flowing NH_3. The precursor powder was heated to the indicated temperature and then cooled in flowing NH_3 prior to FTIR analysis.

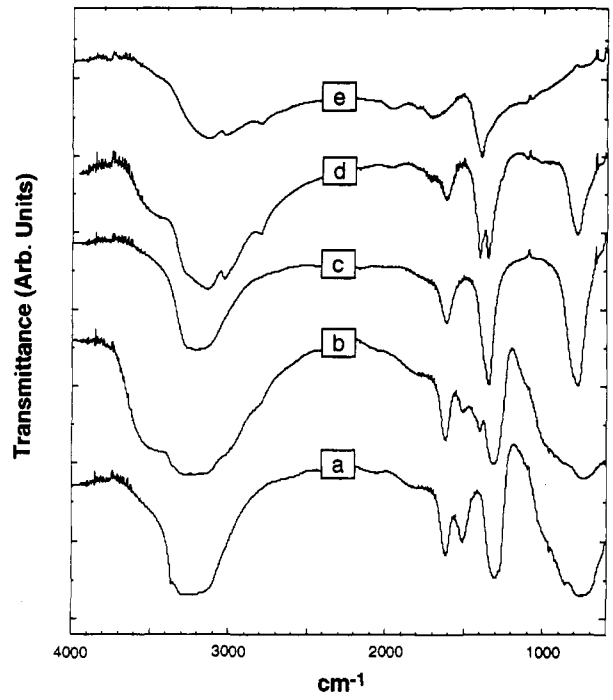

Figure 6. Transmission FTIR spectra: (a) the precursor powder, $[Al(NH_2)(NH)]_n$ and $Al(NH_3)_6Br_3$; (b) the precursor powder after exposure to air for 30 min; (c) an authentic sample of $Al(NH_3)_6Br_3$ prior to exposure to air; (d) $Al(NH_3)_6Br_3$ after exposure to air for 20 min; (e) NH_4Br.

characteristic of symmetric and asymmetric N–H bending modes in NH_3 groups; a broad feature centered at 1513 cm^{-1} that arises from unresolved N–H bending modes in NH_2 and NH groups; and another broad peak at about 3250 cm^{-1} that arises from the N–H stretching modes in NH_3, NH_2, and NH.[7,17,18]

The broad band at 1307 cm^{-1} results from $Al(NH_3)_6Br_3$ and NH_3 loosely coordinated to $[Al(NH_2)(NH)]_n$.[18] Evidence is provided by NMR data discussed later[11] and by an FTIR spectrum of an authentic sample of $Al(NH_3)_6^{3+}$ (Figure 6c). The unresolved peaks centered at 1513 cm^{-1} result from NH_2 and NH in $[Al(NH_2)(NH)]_n$.[7] These assignments are further supported by the change in the relative intensities of the peaks at 1513 and 1620 cm^{-1} upon heating. Prior to heating, the 1513-cm^{-1} band, which results from NH_2 and NH groups, is more prominent than the 1620-cm^{-1} band, which arises from NH_3 groups. After heating to 200 °C, the 1620-cm^{-1} band is dominant, indicating NH_3 condensation from $[Al(NH_2)(NH)]_n$. Moreover, the broad band at 1307 cm^{-1} shifts to 1356 cm^{-1} and becomes much narrower after heating, which may reflect loss of loosely coordinated NH_3 from $[Al(NH_2)(NH)]_n$.[11]

At 400 °C, $Al(NH_3)_6Br_3$ differentially sublimes from the AlN polymer precursor and the peaks at 1620 and 1356 cm^{-1} decrease significantly. Essentially all N–H absorptions are absent after calcining at 1100 °C, including the large N–H stretching feature originally present at about 3250 cm^{-1}. These data, along with the broad Al–N stretching peak at about 800 cm^{-1}, which is present in all of the spectra, are consistent with formation of H-free AlN powder. Importantly, the FTIR data show that most of the chemistry responsible for the precursor-to-ceramic transformation is over by 600 °C, approximately half the temperature required to make AlN by traditional routes (eqs 1 and 2).

Comparison of the spectra shown in Figure 5 with a spectrum of pure NH_4Br (Figure 6e) indicates that all NH_4Br originally present in the cell is consumed by electrochemical reactions prior to calcination, consistent with our earlier contention that NH_4^+ is reduced to NH_3 during the course of the electrolysis.

Although no NH_4Br survives a typical 6–8-h electrolysis, we have occasionally observed it in the precursor powder after exposure to air.[6] This is a result of air-induced conversion of $Al(NH_3)_6Br_3$, and possibly $[Al(NH_2)(NH)]_n$, to NH_4Br. Parts c and d of Figure 6 are the spectra of an authentic sample of $Al(NH_3)_6Br_3$ before and after exposure to air. Comparison of these spectra with that of pure NH_4Br (Figure 6e) clearly indicates partial conversion of $Al(NH_3)_6Br_3$ to NH_4Br; the NH_4^+ peak at 1404 cm^{-1}, which results from an N–H bending mode, is present in the $Al(NH_3)_6Br_3$ spectrum only after exposure to air.[17] There are also shoulders on the peaks of the exposed $Al(NH_3)_6Br_3$ at 2806 and 3039 cm^{-1} that were not present prior to exposure, but which can be traced to the NH_4Br spectrum. A similar trend is observed when the precursor powder is exposed to air. Prior to exposure (Figure 6a), no features are observed in the spectrum that can be attributed to NH_4Br. However, after exposure to air (Figure 6b), a peak at 1404 cm^{-1} is evident as a shoulder on the NH_3 symmetric N–H bending peak at 1307 cm^{-1}, and there are two small peaks at 2806 and 3039 cm^{-1}. All three of these bands arise from NH_4^+ present in the precursor powder only after it is exposed to air. XRD data, discussed later, indicate that NH_4^+ is present as NH_4Br in the precursor powder after it is exposed to air.

Figure 6 also provides information that suggests that $[Al(NH_2)(NH)]_n$ degrades after exposure to air. The band at 1513 cm^{-1}, which arises from NH_2 and NH in $[Al(NH_2)(NH)]_n$, is prominent in the precursor spectrum before exposure to air (Figure 6a), but it is significantly diminished following exposure (Figure 6b). Since no other new peaks appear in Figure 6b (except those attributed to NH_4Br), we conclude that the air-induced degradation product of $[Al(NH_2)(NH)]_n$ is either NH_4Br or a NH_3 condensation product such as species C in Scheme II.

We can summarize the FTIR data as follows: Comparison of a spectrum of the precursor powder prior to calcining with the spectra of NH_4Br and $Al(NH_3)_6Br_3$ indicates the presence of the latter but not the former. In addition, bands attributable to NH_2 and NH, arising from $[Al(NH_2)(NH)]_n$, are also present. Heating in NH_3 decreases, first, the NH_2- and NH-band intensities, indicating NH_3 condensation from the polymer and, second, NH_3-band intensity, indicating NH_3 elimination from both the

(17) Bellamy, L. J. *The Infra-red Spectra of Complex Molecules*; Wiley: New York, 1975.
(18) Nakamoto, K. *Infrared and Raman Spectra of Inorganic and Coordination Compounds*, 3rd ed.; Wiley: New York, 1978; pp 197–199.

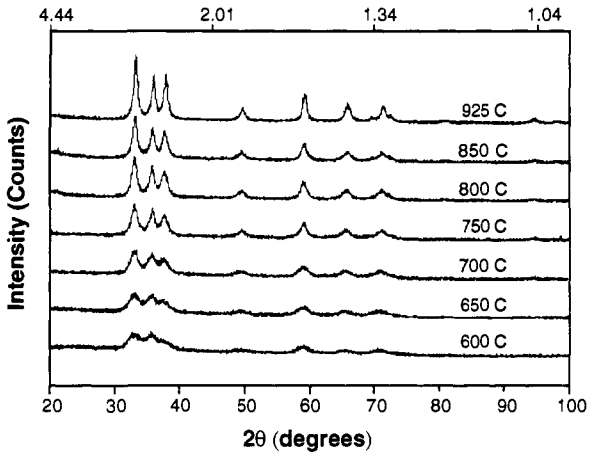

Figure 7. XRD data for the precursor powder calcined at various temperatures in flowing NH_3.

Table II. Summary of the Elemental Composition and Morphological Characteristics of AlN and the Precursor Powder Prepared in a NH_4Br/NH_3 Electrolyte Solution[a]

elemental analysis	precursor powder (wt %)	AlN (wt %)
Al	19.39[b]	66.12 (65.9)
N	35.68	33.92 (34.1)
O	[c]	1.4
C	0.82	<0.5
Br	35.42	<0.5
H	5.65	<0.5
total	97.0 (100)	101.4 (100)
mole ratio, Al/N		1.01 (1.00)
BET surface area (m^2/g)		87
helium density (g/cm^3)		2.97 (3.26)
primary particle diameter (nm)[21]		24
mean crystallite diameter (nm)[22]		12

[a] The precursor powder was calcined at 1100 °C in flowing NH_3. Theoretical values, where appropriate, are listed in parentheses. [b] The Al-anode weight loss corresponding to this experiment was 0.427 g. [c] Oxygen analysis was not obtained for the precursor powder.

AlN polymer precursor[11] and $Al(NH_3)_6Br_3$. After heating to 1100 °C, only bands attributable to AlN are present. Exposure of the precursor powder to air converts some $Al(NH_3)_6Br_3$ to NH_4Br and also eliminates some NH and NH_2 band intensity, suggesting polymer degradation to either NH_4Br or an NH_3 condensate of $[Al(NH_2)(NH)]_n$. Importantly, calcining removes impurities arising from exposure of the powder to air; when the precursor powder is exposed to air for 40 min and then calcined in flowing NH_3 at 1100 °C, XRD and FTIR spectroscopy indicates only the presence of AlN.

X-ray diffraction (XRD) spectra (Figure 7) are consistent with the FTIR analysis. These data show the onset of a crystalline AlN phase at temperatures as low as 600 °C, but there is no evidence for NH_4Br, $Al(NH_3)_6Br_3$, or Al_xO_y phases.[19] The XRD linewidths are also consistent with our previous finding that the calcined precursor powder results in nanophase AlN particles.[6]

Solid-state ^{27}Al magic angle spinning NMR data corresponding to powders calcined at different temperatures are shown in Figure 8. These data indicate that Al present in the precursor powder is essentially all 6-coordinate, since a single absorption is present in the NMR spectrum.[20] When the sample is heated to 200 °C, a partial transition occurs to 4-coordinate Al. Spectra obtained at 600 and 1100 °C are identical and indicate that the transition

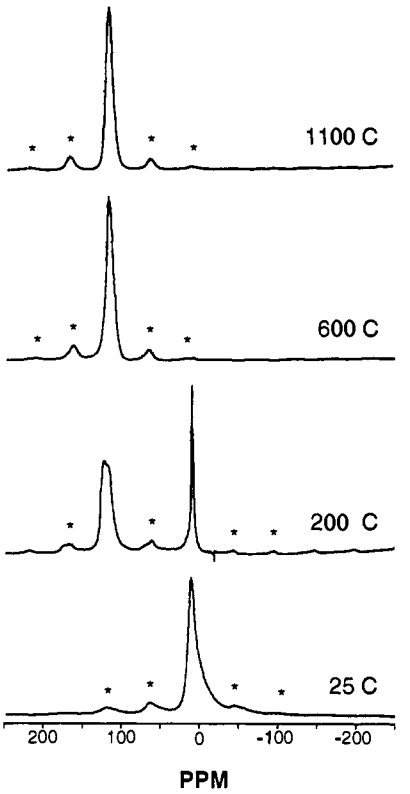

Figure 8. ^{27}Al MAS NMR spectra of the precursor powder before and after calcining in flowing NH_3. The peak in the bottom spectrum is consistent with 6-coordinate Al, and the peak in the top spectrum is consistent with 4-coordinate Al in AlN. The peaks marked with asterisks were confirmed to be spinning sidebands.

to 4-coordinate AlN is complete at 600 °C.[3] Within the detection limit of ^{27}Al NMR, no Al_xO_y phases are observed.

The elemental and morphological analyses of the AlN powder, calcined at 1100 °C in flowing NH_3, and the precursor powder are shown in Table II. The data for the precursor powder are of limited utility, since we are not certain how much NH_3 might be physisorbed onto it. However, the results for AlN clearly indicate the presence of a very pure, stoichiometric AlN powder. There is no evidence for high levels of C or O impurities, consistent with the fact that the powder is never exposed to compounds containing those elements during the course of electrosynthesis and calcination. Moreover, the AlN powder has a very high surface area on the basis of both XRD line width measurements and BET surface area measurements. This suggests, and sintering data discussed later also indicate, that the calcined powder should have a low sintering temperature—a very desirable characteristic of useful AlN powders.[1-3]

The surface area of the powders is a function of the calcining temperature: lower temperatures result in higher surface areas. The primary particle and mean crystallite diameters of the AlN powders calcined at various temperatures in NH_3 are shown in Figure 9. The primary particle diameters were calculated from the measured BET surface area and the theoretical density of AlN.[21] The mean crystallite diameters were calculated from the XRD line widths (Figure 7) and the Scherrer equation.[22] These data indicate that, even under high-temperature calcining conditions, the surface areas are much higher than those of most commercially available powders.[1-3] Moreover, since the primary

(19) *Powder Diffraction File Alphabetical Index, Inorganic Phases*; McClune, W. F., Ed.; JCPDS International Center for Diffraction Data: Swarthmore, PA, 1988. Card Numbers: AlN (25-1133), NH_4Br (5-0618), $Al(NH_3)_6Cl_3$ (28-2), $Al_2O_3 \cdot 3H_2O$ (18-50).

(20) (a) Kinsey, R. A.; Kirkpatrick, R. J.; Hower, J.; Smith, K. A.; Oldfield, E. *Am. Mineral.* **1985**, *70*, 537. (b) Müller, D.; Gessner, W.; Behrens, H.-J.; Scheler, G. *Chem. Phys. Lett.* **1981**, *79*, 59.

(21) The primary particle diameter was calculated from the measured BET surface area and skeletal or theoretical (3.26 g/cm^3) density. Assuming spherical particles, $d = 6/A\rho$, where d is particle diameter, A is the surface area, and ρ is the density.

(22) The Scherrer equation is $D = 0.89\lambda/(B \cos \theta)$, where B is the XRD peak width at half maximum (the AlN(100) peak was used for these calculation), θ is the Bragg angle, and λ is the wavelength of radiation. See: Cullity, B. D. *Elements of X-Ray Diffraction*; Addison-Wesley: Reading, PA, 1978; p 102.

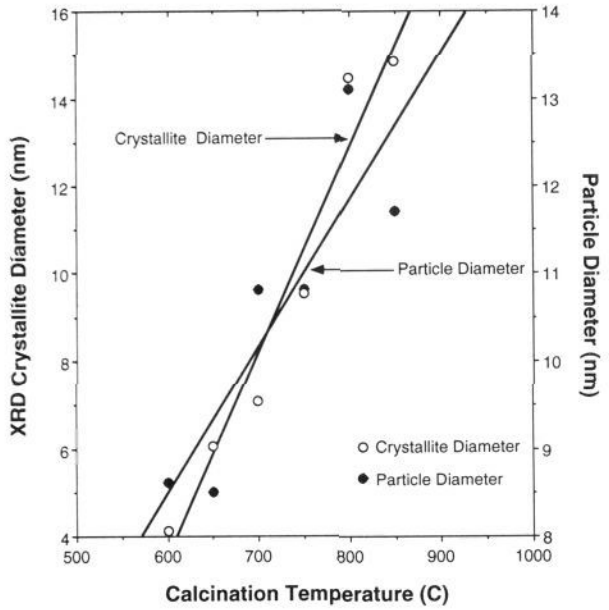

Figure 9. Primary particle diameters (filled circles) and mean crystallite diameters (open circles) of AlN as a function of calcining temperature. Powders were calcined in flowing NH_3. The primary particle diameters were calculated on the basis of the measured BET surface area and the theoretical density of AlN (3.26 g/cm^3).[21] The mean crystallite diameters were calculated from XRD line widths and the Scherrer equation.[22]

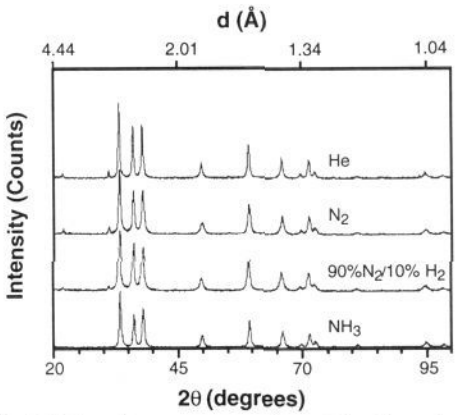

Figure 10. XRD data for precursor powders calcined in various flowing gases at 1000 °C. The minor peaks at $2\theta = 22°$ and 31° in the top three spectra result from NH_4Br impurities.

particle and mean crystallite diameters are similar, we conclude that the crystallites are of uniform size and shape.

We have also examined the effect of the calcining ambient on the purity of AlN powders. Figure 10 shows XRD spectra for AlN powders calcined at 1000 °C in the presence of four different flowing gases. The bottom spectrum was obtained from a precursor sample calcined in flowing NH_3. The diffraction maxima in this spectrum are identical to those reported in the literature for pure AlN.[19] Spectra obtained from samples calcined in He, N_2, and 10% H_2/90% N_2 are very similar to the spectrum of pure AlN, except for small peaks at $2\theta = 22°$ and 31° that are due to NH_4Br.[19] Elemental analyses of the powders used to obtain the spectra shown in Figure 10 provide the following weight-percent oxygen impurities: NH_3 (0.87%), 90% N_2/10% H_2 (1.01%), N_2 (1.25%), He (0.69%).

SEM micrographs (Figure 11) yield additional clues concerning the origin of NH_4Br in the powders not calcined in NH_3. The powders calcined in He, N_2, and 10% H_2/90% N_2 all have closed, low surface area structures. This suggests that NH_4Br, probably formed within AlN crystallites as a consequence of chemical reactions involving Br-containing species present in the precursor powder, is trapped and does not sublime during calcination.

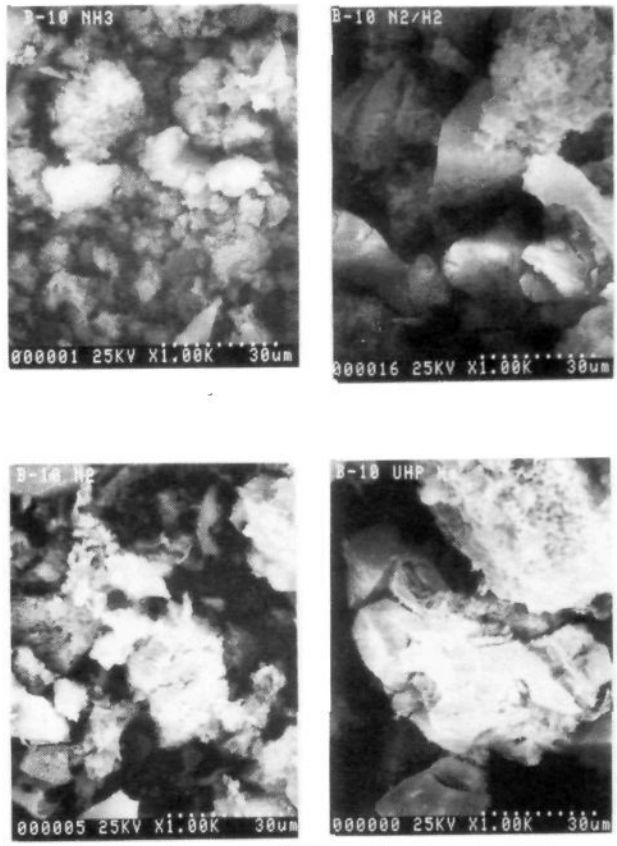

Figure 11. SEM micrographs of AlN powders prepared by calcining the precursor powder in various atmospheres at 1000 °C: (top left) NH_3; (top right) 10% H_2/90% N_2; (bottom left) N_2; (bottom right) He.

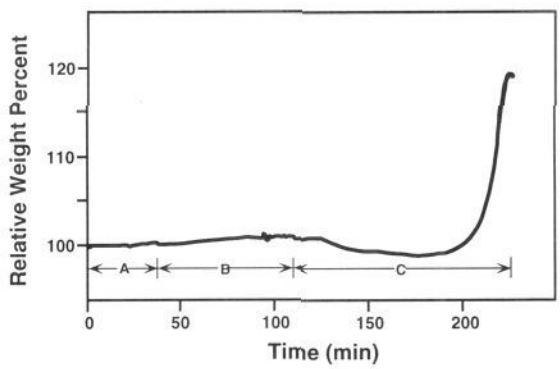

Figure 12. TGA of AlN powder calcined at 1000 °C, then exposed to flowing N_2 at 25 °C (part A) and $O_2 + H_2O$ at 25 °C (part B), and *finally heated in flowing, dry O_2 at 10 °C/min to a final temperature of* 1100 °C (part C). The mass increase present at 1065 °C corresponds to quantitative conversion of AlN to Al_2O_3.

However, when the precursor is calcined in NH_3, the resulting AlN has a much more open structure that permits any NH_4Br that might be present to differentially sublime from the AlN polymer precursor during calcination.

Since commercially available, high surface area AlN powders degrade upon exposure to air as a result of surface oxidation,[1-3,23] we examined the stability of electrochemically prepared AlN in wet and dry O_2 and N_2. These experiments were carried out by exposing a recently calcined powder to a flowing gas stream of either dry N_2 or wet O_2 and then measuring the mass change of the powder as a function of time and temperature. The results indicate that the powders are stable under a wide variety of

(23) Paquette, M. S.; Board, J. L.; Haney, C. N.; Knudsen, A. K.; Susnitzky, D. W.; Rudolf, P. R.; Beaman, D. R.; Newman, R. A.; Froelicher, S. W. *Ceram. Trans.* **1990**, *12*, 855.

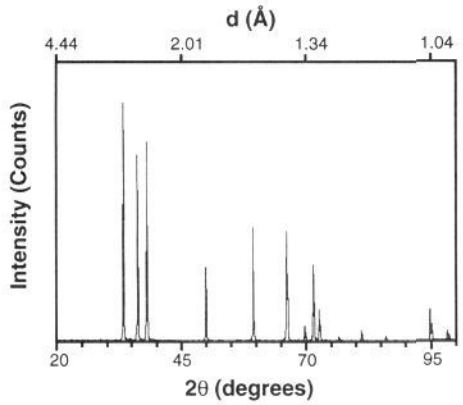

Figure 13. XRD spectrum for AlN powder hot-pressed at 1800 °C and 1500 psi in O_2-gettered Ar for 1 h without sintering aids.

conditions. Figure 12 shows the result obtained when first N_2 and then wet O_2 are passed over AlN powder at 25 °C. Importantly, no mass changes result except for a small increase during the period that the sample was exposed to wet O_2. When the powder is heated in dry O_2, the water adsorbed during the previous cycle desorbs at about 100 °C. The AlN powder is stable in dry O_2 to about 800 °C before it is quantitatively converted to Al_2O_3 at about 1065 °C. The important result is that these very high surface area powders resist surface oxidation under a range of ambient conditions, in contradistinction to powders prepared by other routes.[1-3,23] Since the presence of surface oxide phases degrades thermal conductivity and necessitates the use of additives to getter lattice oxygen to grain boundaries at normal processing temperatures, this is a significant observation.

We have made some preliminary sintering studies, and the resulting data are presented here. A full sintering study will appear elsewhere.[24] AlN powders calcined at 1000 °C in flowing NH_3 were hot-pressed at 1800 °C and 1500 psi for 1 h in O_2-gettered Ar. After pressing, the material was 97% densified and translucent. More recent data indicate that hot pressing at 1600 °C and 5000 psi for 2 h in O_2-gettered Ar results in fully dense material. The XRD spectrum of the material sintered at 1800 °C (Figure 13) indicates that the mean crystallite size increases but that no impurities are present in the sintered powder within the sensitivity of XRD. SEM micrographs (Figure 14) indicate a 2–5-μm crystallite size. Elemental analysis shows that the O_2 impurity level after calcining without sintering aids amounts to 0.9%. Thermal conductivity measurements of the sintered material are presently underway.[24]

Conclusions

We have shown that a simple electrochemical apparatus consisting of two Al electrodes and an NH_4Br/NH_3 electrolyte solution can be used to generate an inorganic AlN polymer precursor. Calcination of this material in flowing NH_3 at 600 °C results in fully crystalline AlN; heating above 600 °C only results in crystal growth. Elemental analysis of the crystalline material indicates

(24) Garza, E. G.; Wade, T.; Smith, D. M.; Crooks, R. M. Manuscript in preparation.

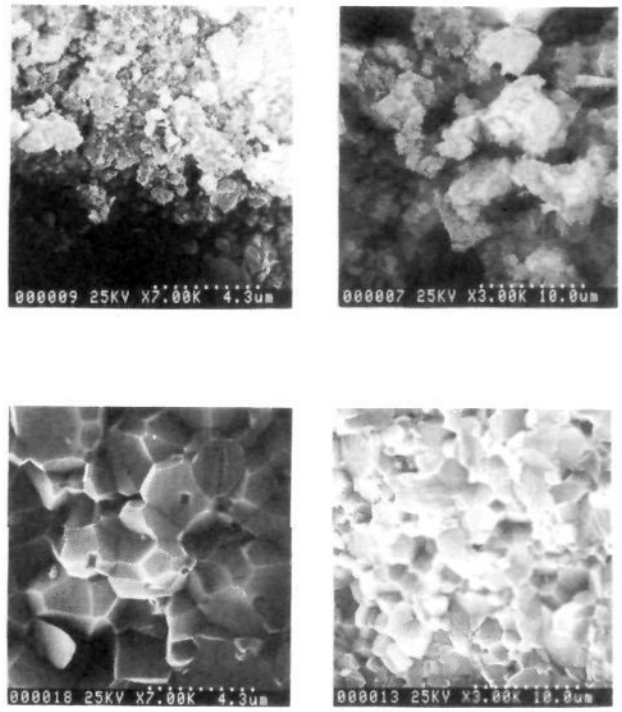

Figure 14. SEM micrographs of AlN powders prepared by calcining the precursor powder in flowing NH_3 at 1100 °C: before (top) and after (bottom) hot pressing at 1800 °C and 1500 psi in O_2-gettered Ar.

that it is largely free of C and O impurities. The high surface area powder fully densifies when hot-pressed at 1600 °C and 5000 psi to yield 2–5-μm crystallites. Previously, we have shown that this technique is appropriate for synthesizing other metal nitride ceramics such as TiN.[6] More recently, we have used this electrochemical route to synthesize phase-pure Zn_3N_2 and NbN.

Experiments are presently underway to fully reveal the mechanistic chemistry that leads to AlN, improve cell current efficiency, and construct a small-scale flow reactor. Results obtained from these experiments will be reported separately.

We believe that the electrochemical-based synthesis of AlN reported here represents one of the first major contributions of electrochemistry to materials chemistry, and we anticipate that it will serve as a paradigm for future research.

Acknowledgment. This work has been partially supported by the UNM/NSF Center for Micro-Engineered Ceramics, a collaborative effort supported by NSF (Grant CDR-8800352), Los Alamos and Sandia National Laboratories, the New Mexico Research and Development Institute, and the ceramics industry. Acknowledgment is made to the donors of the Petroleum Research Fund, administered by the American Chemical Society, for partial support of this research. We thank Dr. Kevin Howard and Ms. B. Lynn Stiehl of the Dow Chemical Company for providing some of the elemental analysis data. The ^{27}Al NMR spectroscopy was performed by Dr. Yong Wah Kim and Dr. Andrea Labouriau of Los Alamos National Laboratory.